Magnetic self-assembly of three-dimensional surfaces from planar sheets

Mila Boncheva*, Stefan A. Andreev*, L. Mahadevan†, Adam Winkleman*, David R. Reichman‡, Mara G. Prentiss§, Sue Whitesides¶, and George M. Whitesides*‖

*Department of Chemistry and Chemical Biology, Harvard University, 12 Oxford Street, Cambridge, MA 02138; †Division of Engineering and Applied Sciences, Harvard University, 29 Oxford Street, Cambridge, MA 02138; ‡Department of Chemistry, Columbia University, 3000 Broadway, New York, NY 10027; §Department of Physics, Harvard University, 17 Oxford Street, Cambridge, MA 02138; and ¶School of Computer Science, McGill University, 3480 University Street, Montreal, QB, Canada H3A 2A7

Contributed by George M. Whitesides, February 1, 2005

This report describes the spontaneous folding of flat elastomeric sheets, patterned with magnetic dipoles, into free-standing, 3D objects that are the topological equivalents of spherical shells. The path of the self-assembly is determined by a competition between mechanical and magnetic interactions. The potential of this strategy for the fabrication of 3D electronic devices is demonstrated by generating a simple electrical circuit surrounding a spherical cavity.

folding | microfabrication | 3D structure | soft lithography | soft electronics

The strategies used to form 3D micro- and nanostructures in cells and by humans differ. Proteins, RNAs, and their aggregates, the most complex, 3D molecular structures in nature, form by the spontaneous folding of linear precursors (1). The ubiquity of this strategy reflects the efficiency with which the cell synthesizes linear precursors by sequential formation of covalent bonds. Microelectronic devices, the most complex 3D structures generated by humans, are fabricated by stacking and connecting planar layers (2). This strategy is dictated by the availability of highly developed methods for parallel microfabrication in 2D and the absence of effective, general methods for fabrication in 3D (3).

Folding of connected, 2D plates [using robotics (4) or spontaneous folding (5–9)] can yield 3D microelectromechanical systems (MEMS) and microelectronic devices. We (10, 11) and others (4, 12) have explored a number of routes to small 3D shapes based on self-assembly. These strategies are still early in their development.

Here, we explore a new strategy for formation of 3D objects that combines the advantages of planar microfabrication with those of 3D self-assembly. Our approach comprises four steps (Fig. 1*a*): (*i*) cutting the 3D surface of interest into connected sections that "almost" unfold into a plane (unpeeling a sphere as one unpeels an orange is an example); (*ii*) flattening this surface and projecting it onto a plane; (*iii*) fabricating the planar projection in the form of an elastomeric membrane patterned with magnetic dipoles; and (*iv*) allowing this patterned membrane to fold into an "almost-correct" 3D shape by self-assembly. This strategy offers the potential to transform easily patterned, functionalized planar sheets into 3D structures and devices. It also raises the problem of designing and generating stable 3D structures by decomposing and projecting these structures into 2D shapes and then balancing the shapes of 2D cuts, the placement of magnetic dipoles, and the mechanical characteristics of the membrane.

Converting sheets into 3D objects by folding and creasing is a very old, remarkably interesting, and still incompletely resolved problem in applied mathematics (13–16). The inverse problem—mapping the surface of a 3D shape (specifically, the surface of the Earth) onto a flat sheet—has been at the core of cartography since the times of Frisius (1508–1555) and Mercator (1512–1594). Although it is known that a flat, inextensible surface cannot fold into a surface that is curved along two orthogonal axes (17), an exhaustive list of the necessary and sufficient conditions to fold a planar sheet into a given 3D shape still remains to be compiled. Theoretical work and modeling have focused on folding of square sheets without slits (18), on approximating 3D surfaces with tessellations (19, 20), and on almost developable conical deformations (21).

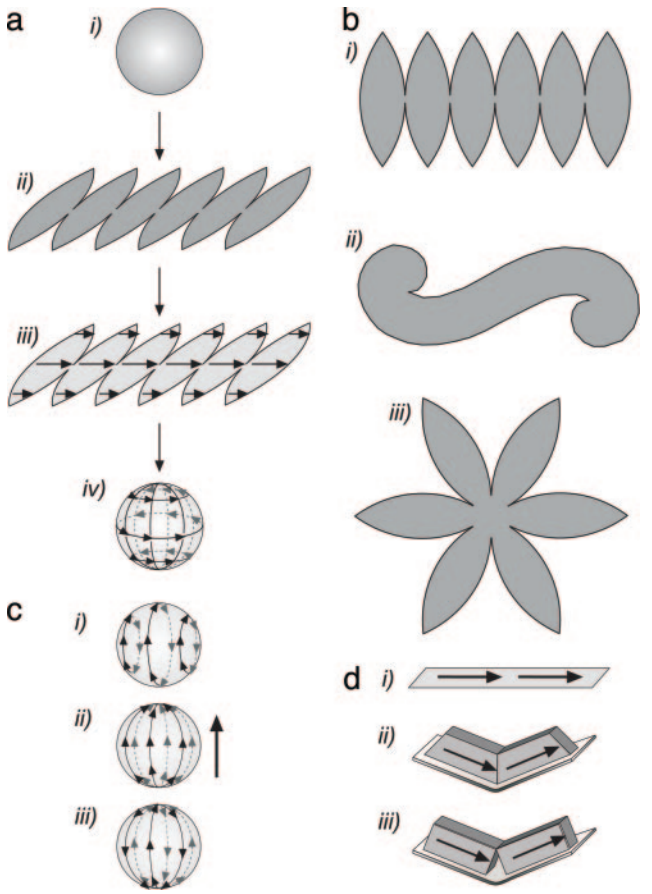

Fig. 1. Design of flat, planar sheets intended to fold into spherical shells. (*a*) Scheme illustrating the general approach explored in this work (see text for details). The magnetic dipoles patterned on the elastomeric sheets are shown with arrows. The design parameters we focused on were the 2D shape of the flat sheets (illustrated in *b*), the pattern of magnetic dipoles in the folded structures (illustrated in *c*), and the shape of the magnetized features (illustrated in *d*).

Abbreviations: LED, light-emitting diode; PDMS, poly(dimethylsiloxane).

‖To whom correspondence should be addressed. E-mail: gwhitesides@gmwgroup.harvard.edu.

www.pnas.org/cgi/doi/10.1073/pnas.0500807102

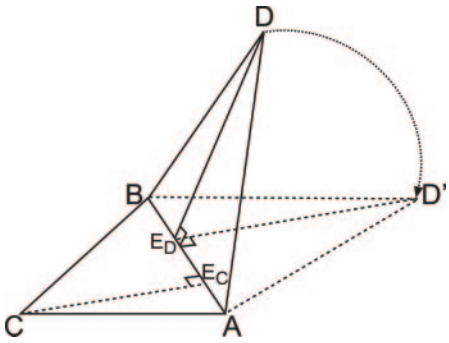

Fig. 2. Scheme illustrating the unfolding of two adjoining, triangular faces of a polytope (ABC and ABD) by mapping the point D to point D′ in the plane of the triangle ABC.

Folding a planar sheet into a surface that is curved locally along two orthogonal axes causes the middle surface of the sheet to be stretched because of changes in the Gaussian curvature (22). Because stretching a sheet is energetically more expensive than bending it, we minimized the geometric incompatibilities between the planar and the 3D forms by using appropriately shaped, 2D, soft, elastomeric membranes. We chose magnetic forces to guide the self-assembly for three reasons: (*i*) magnetic interactions are insensitive to the surrounding medium and to the details of surface chemistry (8); (*ii*) the distances over which they act can be engineered to cover a range of sizes (nanometers to meters); and (*iii*) magnetic dipoles tend to form stable closed loops, and these loops are features easily translated into design rules (23).

Design of 2D Elastomeric Sheets Patterned with Magnetic Dipoles

Our initial efforts at design have been subjective and empirical. We tried to achieve a compromise among five factors: (*i*) the strain introduced upon folding; (*ii*) the fidelity with which the folded sheet reproduced the target structure; (*iii*) the maximization of the favorable magnetic interactions; (*iv*) the ease of fabrication; and (*v*) the potential for embedding and interconnecting electrical circuit elements.

We explored elastomeric sheets having three different 2D shapes: an equatorial cut (Fig. 1*bi*), an orange-peel cut (Fig. 1*bii*), and a flower-petal cut (Fig. 1*biii*). We generated the shapes of the flat sheets by using a modified version of the software package UNFOLD POLYTOPE for MATHEMATICA (www.cs.mcgill.ca/~fukuda/download/mathematica). In the original package, a polytope (specified as a collection of faces and edges) is unfolded by cutting a number of edges and rotating the faces around the remaining edges until they all lie in the same plane. Fig. 2 illustrates the unfolding process for one vertex, D. The new location, D', of the vertex, D, is calculated as

$$\overrightarrow{E_D D'} = \overrightarrow{CE_C}\frac{|\overrightarrow{E_D D}|}{|\overrightarrow{CE_C}|}.$$

We modified some routines of the software package so that we could specify the positions of the cuts and avoid mistakes during the unfolding process. Fig. 3 shows three stages of the unfolding of this polytope into a 2D pattern comprising six segments (flower-petal cut; see Fig. 1*biii*). First, we created a polytope approximating a sphere. The unfolding started by selecting one polygon as a center and specifying radial cuts away from it. A tree of faces was thus generated, with the central polygon located at the top and the faces at the ends of the cuts located at the bottom of the polytope. The polygons were then unfolded as shown in Fig. 3.

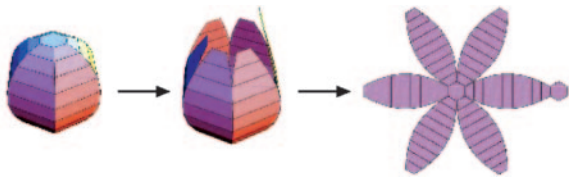

Fig. 3. Scheme illustrating three stages of unfolding of a polytope approximating a sphere into a flat surface shaped as the flower-petal cut.

We examined three different patterns of magnetic dipoles: the patterns in Fig. 4 *a* and *e* were designed to form spheres containing closed loops of magnetic dipoles parallel to one another (Fig. 1*ci*), the pattern in Fig. 4*c* was designed to form a sphere containing six rows of dipoles connecting at magnetically opposite poles (Fig. 1*cii*), and the pattern in Fig. 4*g* was designed to form a sphere containing three closed loops of dipoles that cross one another at the two poles at an angle of 120° (Fig. 1*ciii*). By optimizing the shape of the magnetized blocks, it was also possible to use steric interactions between them to stabilize the folded structures (Fig. 1*d*).

Results and Discussion

Folding of Elastomeric Sheets. Self-assembly took a different course in these four cases. The magnetically patterned sheet shown in Fig. 4*a* folded into a sphere (Fig. 4*b*) either during peeling from the support or after mild agitation for 1–2 min in water. The equatorial magnetic loop closed first, followed immediately by the loops at the poles. The sheet shown in Fig. 4*c* always folded into the structure shown in Fig. 4*d* but only after vigorous agitation for 2–13 min in water. The sheet shown in Fig. 4*e* almost always folded incorrectly when suspended in water: Sections facing one another in the planar sheet interacted through their larger magnetic features. This precursor, however, folded correctly when we guided the self-assembly process by placing the sheet at the air–water interface (rather then suspending it in water), with the magnets facing down. Gravity brought sections adjacent in the flat sheet into close contact out-of-plane, and the sheet formed a sphere after 1–2 min of mild agitation (Fig. 4*f*). The precursor shown in Fig. 4*g* did not fold into a sphere under any experimental conditions (Fig. 4*h*).

Finite-Element Simulation of Magnetic Field Profiles. We performed a finite-element simulation of the 2D magnetic field profiles of the unfolded flat precursors and of cross sections of the folded 3D structures by using the software package FINITE ELEMENT METHOD MAGNETICS (http://femm.foster-miller.com). We set the magnetic field intensity at the surface of each magnet to 0.04 T (the experimentally measured upper limit) and treated the poly(dimethylsiloxane) (PDMS) membrane as a diamagnetic material with the magnetic characteristics of air (a preset feature of the software). From an input of the shape of the flat sheet (or a cross section of the 3D structure) patterned with magnetic features of given shape, polarity, and magnetic permeability, this software calculates and maps the magnetic field intensity and the magnetic field lines. In the output of the simulation, the intensity of the magnetic field is depicted by color intensity: Higher field intensity corresponds to a darker shade of gray. The strength of the interactions between the patterned magnets can be estimated from the strength of the magnetic field and the number of field lines in the space surrounding the magnets. Thus, a magnetic energy minimum corresponds to a map in which the field intensity and the field lines are confined only to the regions of high magnetic permeability (i.e., within the magnets) and do not extend (or extend only to a negligible degree) into the regions of

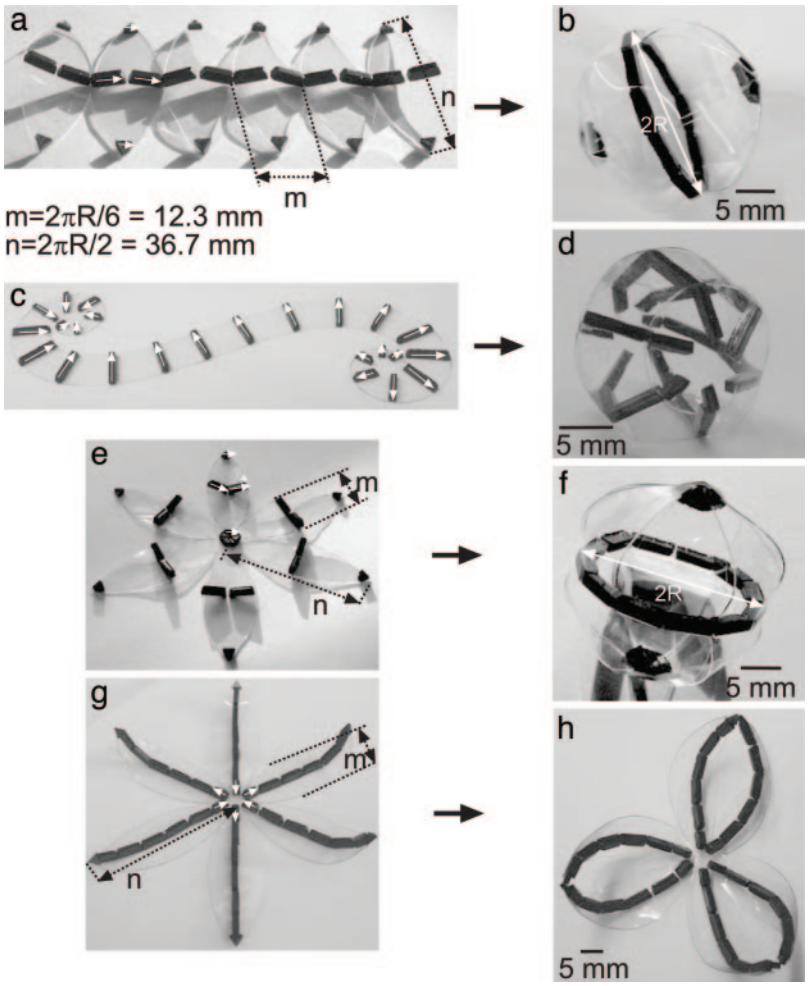

Fig. 4. Three-dimensional structures (*b*, *d*, *f*, and *h*) self-assembled from magnetically patterned sheets (*a*, *c*, *e*, and *g*). The direction of the magnetic dipoles in the magnetized, PDMS features is indicated with white arrows. See supporting information, which is published on the PNAS web site, for details of design, fabrication, and self-assembly of the patterned sheets.

low magnetic permeability (i.e., in the plane of the elastomeric membrane, outside of the magnets).

Fig. 5 shows the results of the simulation. In the unfolded equatorial cut (Fig. 5*a*), there were significant interactions between adjacent magnets positioned in the middle of the segments. No interactions were observed between the magnets positioned at the tips of the segments and between magnets positioned in the middle and at the tips of each segment. In the unfolded flower-petal cut (Fig. 5*b*), there was appreciable interaction between the magnets positioned in the middle of the segments. The central region containing six triangular magnets formed a completely closed ring of magnetic dipoles and showed no stray field lines extending away from the magnets. There was no interaction between magnets positioned at the tips of adjacent sections of the membrane; there was also no interaction between those magnets and the magnets positioned in the middle of the segments. Upon folding of both the equatorial cut and the flower-petal cut, the magnets positioned at the tips of the segments (Fig. 5*e*) and the magnets positioned in the middle of the segments (Fig. 5*f*) formed continuous, closed rings of magnetic dipoles; the field intensity and the field lines in these areas were confined exclusively within the rings, indicating minimized magnetic energy of the folded structures.

In the orange-peel cut (Fig. 5*c*), the simulation showed interactions only between magnets positioned at the two ends of the sheet. In a vertical cross section of the folded structure (Fig. 5*g*), the simulation indicates the presence of an overall net dipole moment between the two poles.

The flower-petal cut patterned with magnets arranged antiparallel to one another (Fig. 5*d*) did not form a sphere; it folded, instead, into stable structures comprising groups of two or four petals (see Fig. 4*h*). Fig. 5 *h* and *i* shows simulations of an aggregate comprising three pairs of magnetized features and an aggregate comprising one pair and a group of four magnetized features, respectively. These aggregates correspond to cross sections of the polar regions of a sphere formed from the flower-petal cut shown in Fig. 5*d*, in which the groups of two or four magnetized features are separated by a gap of 400 μm. The simulation shows that the field intensity in these gaps is very low or equal to zero; the dipoles aggregated in pairs or in a group of four have formed closed, (magnetically) stable loops. The energy gain of bringing these small loops into a single loop comprising all six segments would be insignificant compared with the energy gain in the case of a flower-petal cut patterned with equatorially magnetized features (as the one shown in Fig. 5*e*).

Estimation of the Elastic and Magnetic Free Energy of the Folded Structures. The process of folding minimizes the sum of the elastic and magnetic energies of the system: The increase in mechanical energy that occurs on folding the elastic sheet is balanced by the

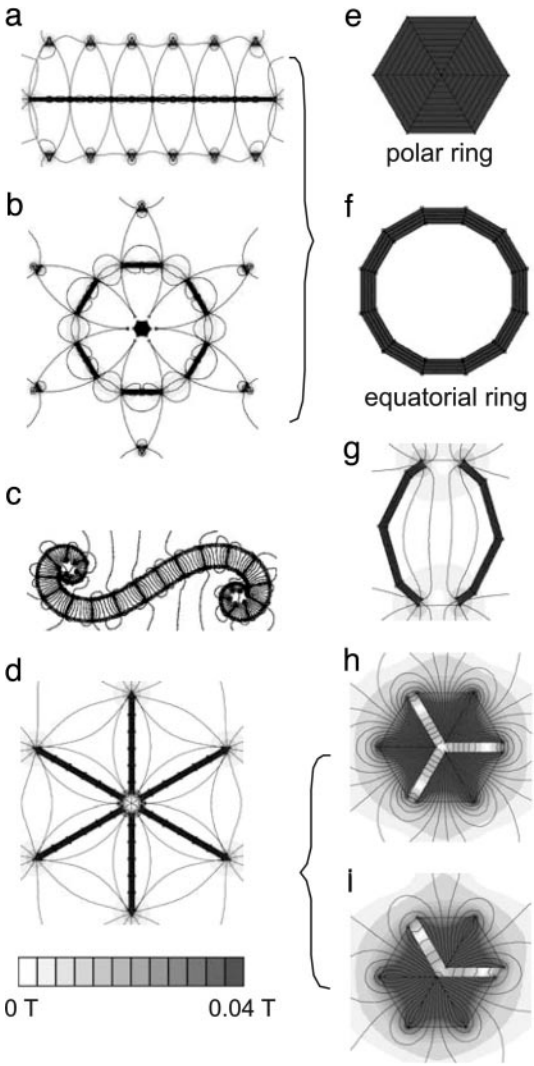

Fig. 5. Results of the finite-element simulation of magnetic field profiles of unfolded, flat patterned sheets (*a–d*) and cross sections of the corresponding folded 3D structures (*e–i*). The magnetic field intensity is represented by the color intensity: higher intensity corresponds to darker shade of gray. The scheme is not to scale.

decrease in magnetic energy as the magnetic dipoles approach one another. We used the balance of the two energies to estimate how changing the size of the components and the thickness of the elastic membrane affects the stability of folded structures. We compared the magnetic energy gained in bringing noninteracting magnetic dipoles into the equatorial loop of the structure shown in Fig. 4 *a* and *b* with the elastic energy cost for bending the sheet around that loop.

To estimate the elastic energy of the system, as a first approximation we considered only the bending energy, U_b, needed to bend a sheet of thickness h made of a material with Young's modulus E into a cylinder by using magnets of length R placed in the middle of the segments. Thin elastic sheets are most easily folded by isometric bending of the middle surface, without stretching it (24); here, we ignored the contribution of the stretching energy that arises because of the presence of boundary layers at ridges (25, 26) and peaks (21, 27). Thus, the elastic energy scales as

$$U_b \sim Eh^3\kappa^2 A, \qquad [1]$$

where $\kappa \sim 1/R$ is the local mean curvature at the center of the sheet and $A \sim R^2$ is its area. The elastic energy due to bending alone is largely independent of the radius of the sphere.

To estimate the magnetic energy of the system, we approximated the magnetic field generated by permanent magnets of length L (proportional to the radius of the sphere) and square cross section b with the field generated by a finite, current-carrying solenoid (28). The magnetic field, $B_{isolated}$, inside each isolated magnet in the unfolded configuration can be described as the magnetic field along the axis of the finite solenoid:

$$B_{isolated} \sim M_0\left(\frac{z}{\sqrt{z^2+b^2}} - \frac{z-L}{\sqrt{(z-L)^2+b^2}}\right), \qquad [2]$$

where M_0 is the magnetic strength of the material, z is the distance from the point at which we measure the field to the face of the solenoid, L is the length of the solenoid, and b is its radius (proportional to the width of the magnets). To estimate the magnetic field, B_{ring}, of the folded configuration, we made the approximation that the magnetic field inside the ring of magnets is constant (similar to the field inside a solenoid torus); thus, it can be expressed (28) as

$$B_{ring} \sim 2M_0. \qquad [3]$$

Using Eqs. **2** and **3**, we can express the change of the magnetic energy, U_m, between the unfolded and the folded configurations as

$$U_m \propto M_0^2 \int_V B_{ring}^2 - B_{isolated}^2 \, dV, \qquad [4]$$

where the integration is done over the volume, V, of the magnets. We calculated the magnetic energy difference due to folding numerically, for the limiting case of $L \gg b$, as

$$U_m \propto M_0^2 \int_V B_{ring}^2 - B_{isolated}^2 \, dV \propto M_0^2 b^3 \tan^{-1}\left(\frac{L}{b}\right). \qquad [5]$$

This rough estimation of the magnetic energy ignores the shape of the closed ring of magnets (in the structures considered in this work, the ring is shaped as a polygon and not as a circle), the variation of the magnetic field away from the main axis of the solenoid, and the magnetic energy outside the volume of the magnets. Nevertheless, the scaling of the magnetic energy with the dimensions of the magnets is largely independent of these effects.

Using Eqs. **1** and **5**, we can then express the balance of the magnetic and elastic energies as

$$\frac{U_m}{U_b} \propto \frac{M_0^2 b^3 \tan^{-1}\left(\frac{L}{b}\right)}{Eh^3\kappa^2 A}. \qquad [6]$$

It is readily apparent that the ratio U_m/U_b depends on the ratios M_0^2/E, b/h, and L/b. The ratio M_0^2/E describes properties of the materials used (magnets and elastic sheets) and does not depend on the dimensions of the folded structure. Using the ratios b/h and L/b, we can estimate how changing the dimensions of the components and the thickness of the elastic membrane will affect the stability of a folded structure: If the width and the length of the magnets are rescaled by a factor α, the thickness of the elastic sheet must be rescaled by the same factor to preserve the balance of the two energies and, thereby, the stability of the folded structure.

An important factor that this simple calculation does not take into account is the possibility of coexistence of several stable, folded shapes for a given set of parameters. The next step in refining the

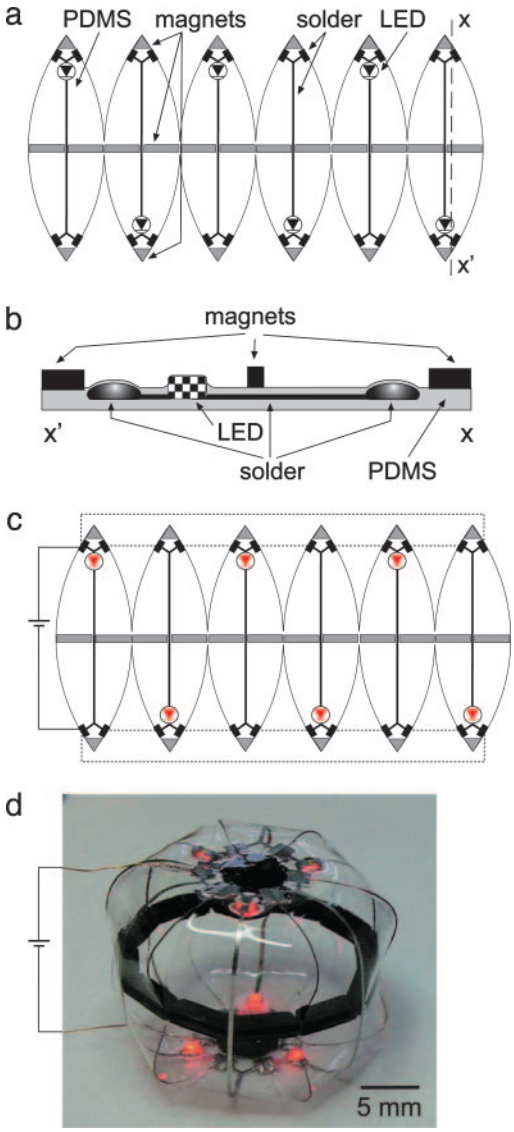

Fig. 6. Self-assembly of a simple electrical circuit surrounding a spherical cavity. (*a* and *b*) Schemes of the patterned, planar sheet before self-assembly, in top view and cross section along x–x′, respectively. (*c*) Self-assembly generates parallel electrical connections between the six light-emitting diodes (LEDs). The solder wires are shown as thick solid lines, the copper wires connecting the self-assembled structure to a battery as thin solid lines, and the electrical connections formed between the LEDs during self-assembly as thin dotted lines. (*d*) Photograph of the self-assembled spherical structure connected to a battery.

scaling estimate will include studies of the energy landscape of the folded structures and the kinetics of the folding process.

Three-Dimensional Electrical Circuit. We used this strategy to generate elementary 3D electrical circuit (Fig. 6). We fabricated each section of a sheet having the design shown in Fig. 6*a* to include an electrically isolated wire (see supporting information for fabrication details). This wire connected the cathode and the anode of a LED to two pairs of solder pads placed at the tips of each section, near the edge of the membrane; these solder pads were intended to provide electrical connectivity between LEDs placed on adjacent sections of the sheet. The solder features (wires and contact pads) were embedded within the PDMS membrane, with the wires close to the middle surface of the sheet that is not stretched when rolled into a cylindrical surface (29, 30) (Fig. 6*b*). When cutting the sheet to shape, we cut through the outside edges of the embedded solder pads and, thus, produced four edges exposing bare solder adjacent to the magnets at the tips of each section. For self-assembly, we suspended the sheet in water at 60°C (the melting temperature of the solder was 47°C) and agitated gently. Within 1–3 min, the planar sheet folded into a sphere; simultaneously, electrical connections formed between the six sections by fusion of the drops of molten solder (Fig. 6*c*). The heat also restored the electrical continuity of wires that had broken during bending of the flat sheet. After self-assembly was complete, and the resulting structure had cooled to room temperature and dried, we connected one top and one bottom contact pad to a battery. Fig. 6*d* shows that all six LEDs illuminate and demonstrates the continuity of an electrical circuit that traces a path through all six sections of the structure.

Conclusions

This work describes an intriguing new strategy for formation of 3D structures starting with 2D sheets and suggests a new route to 3D electrical circuits. It combines concepts extracted from biology (e.g., self-assembly, folding of flexible precursors in 3D, and stabilization of 3D structures by dipole–dipole interactions) with processes and objects familiar from the world of man-made fabrication (e.g., planar patterning, elastomeric polymer membranes, and formation of closed loops of magnetic dipoles).

This work also identifies a remarkably interesting problem in applied mathematics: the analytical design of planar sheets that can fold into 3D structures with minimized global (magnetic and mechanical) free energy. Answering the core question—how to translate a global goal (designing and generating a stable 3D structure) into local interactions defined by the shape of the 2D cut, the placement of the magnetic dipoles, and the mechanical characteristics of the membrane—will require further development in both fabrication and applied mathematics.

This approach combines the efficient methods of photo- and soft lithography for fabrication of flat, patterned surfaces with self-assembly to form 3D from 2D structures. It can be generalized to other interactions (e.g., interactions between patterned electrical monopoles or dipoles, and capillarity) and to a broad range of materials. This strategy is relevant to the fabrication of "soft" electronics (31) (e.g., displays, thin film transistors, and sensor skins) and deployable structures (32). The most immediate problem that should be solved in moving toward applications is to improve the method of fabrication of the precursor membranes. In principle, both fabricating the sheet (with embedded electrical components) and patterning the magnetic dipoles can be accomplished by using planar microfabrication (33, 34).

We thank A. R. Urbach and J. C. Love for help in initiating this project, D. A. Bruzewicz for assisting in the fabrication of patterned flat sheets, and R. Nagpal (Massachusetts Institute of Technology, Cambridge) for helpful discussions on folding. This work was supported by National Science Foundation Grant CHE-0101432 (to M.B., A.W., and G.M.W.), the Defense Advanced Research Planning Agency (M.B., A.W., and G.M.W.), the Office of Naval Research Young Investigator Program (L.M.), the Alfred P. Sloan Foundation (D.R.R.), and a Camille Dreyfus Teacher–Scholar Award (to D.R.R.).

1. Alberts, B., Bray, D., Lewis, J., Raff, M., Roberts, K. & Watson, J. D. (1994) *Molecular Biology of the Cell* (Garland, New York).
2. Gandghi, S. K. (1994) *VLSI Fabrication Principles* (Wiley, New York).
3. Campbell, S. A. (2001) *The Science and Engineering of Microelectronic Fabrication* (Oxford Univ. Press, New York).
4. Balde, J. W. (2003) in *Emerging Technology in Advanced Packaging* (Kluwer Academic, Boston).
5. Syms, R. R. A. & Yeatman, E. M. (1993) *Electron. Lett.* **29,** 662–664.
6. Smela, E., Inganäs, O. & Lundstrom, I. (1995) *Science* **268,** 1735–1738.
7. Vaccaro, P. O., Kubota, K. & Aida, T. (2001) *Appl. Phys. Lett.* **78,** 2852–2854.

8. Son, I. & Lal, A. (2002) in *Proceedings of the Second Annual International IEEE–EMBS Special Topic Conference on Microtechnologies in Medicine and Biology*, eds. Dittmar, A. & Beebe, D. (IEEE, Piscataway, NJ), pp. 332–336.
9. Krulevitch, P., Lee, A. P., Ramsey, P. B., Trevino, J. C., Hamilton, J. & Northrup, M. A. (1996) *J. Microelectromech. Syst.* **5,** 270–282.
10. Boncheva, M., Bruzewicz, D. A. & Whitesides, G. M. (2003) *Pure Appl. Chem.* **75,** 621–630.
11. Whitesides, G. M. & Boncheva, M. (2002) *Proc. Natl. Acad. Sci. USA* **99,** 4769–4774.
12. Syms, R. R. A., Yeatman, E. M., Bright, V. M. & Whitesides, G. M. (2003) *J. Microelectromech. Syst.* **12,** 387–418.
13. Duerer, A. (1977) *The Painter's Manual* (Abaris, New York); translated from a 1525 manuscript by W. L. Strauss.
14. O'Rourke, J. (2000) *Lect. Notes Comput. Sci.* **1763,** 258–266.
15. Dritschel, D. G. & Perkins, R. J. (1996) *The Mathematics of Deforming Surfaces* (Oxford Univ. Press, London).
16. Cerda, E., Mahadevan, L. & Pasini, J. M. (2004) *Proc. Natl. Acad. Sci. USA* **101,** 1806–1810.
17. Eisenhart, L. P. (1909) *A Treatise on the Differential Geometry of Curves and Surfaces* (Ginn and Company, New York).
18. Nagpal, R. (2001) Ph.D. Thesis (Massachusetts Institute of Technology, Cambridge, MA).
19. Demaine, E. D., Demaine, M. L. & Mitchell, J. S. B. (2000) *Computational Geometry: Theory and Applications* **16,** 3–21.
20. Lang, R. J. (1996) *Proceedings of the Twelfth Annual Symposium on Computational Geometry* (ACM, New York), pp. 98–105.
21. Cerda, E., Chaieb, S., Melo, F. & Mahadevan, L. (1999) *Nature* **401,** 46–49.
22. Love, A. E. H. (1944) *A Treatise on the Mathematical Theory of Elasticity* (Dover, New York).
23. Love, J. C., Urbach, A. R., Prentiss, M. G. & Whitesides, G. M. (2003) *J. Am. Chem. Soc.* **125,** 12696–12697.
24. Rayleigh, J. W. S. (1945) *The Theory of Sound* (Dover, New York).
25. Lobkovsky, A., Gentges, S., Li, H., Morse, D. E. & Witten, T. A. (1995) *Science* **270,** 1482–1485.
26. Lobkovsky, A. E. (1996) *Phys. Rev. E* **53,** 3750–3759.
27. Cerda, E. & Mahadevan, L. (1998) *Phys. Rev. Lett.* **80,** 2358–2361.
28. Purcell, E. M. (1985) *Electricity and Magnetism* (McGraw–Hill, New York).
29. Loo, Y.-L., Someya, T., Baldwin, K. W., Bao, Z., Ho, P., Dodabalapur, A., Katz, H. E. & Rogers, J. A. (2002) *Proc. Natl. Acad. Sci. USA* **99,** 10252–10256.
30. Suo, Z., Ma, E. Y., Gleskova, H. & Wagner, S. (1999) *Appl. Phys. Lett.* **74,** 1177–1179.
31. Service, R. F. (2000) *Science* **287,** 415–417.
32. Pellegrino, S., ed. (2001) *CISM International Centre for Mechanical Sciences Courses and Lectures* (Springer, Vienna), No. 412.
33. Choi, K. M. & Rogers, J. A. (2003) *J. Am. Chem. Soc.* **125,** 4060–4061.
34. Cho, H. J., Bhansali, S. & Ahn, C. H. (2000) *J. Appl. Phys.* **87,** 6340–6342.

Supplementary Information

1. Design of the 2D shape of the flat, elastomeric sheets. We generated the shapes of the flat sheets using a modified version of the software package *Unfold Polytope* for Mathematica[1]. In the original package, a polytope—specified as a collection of faces and edges—is unfolded by cutting a number of edges and rotating the faces around the remaining edges until they all lie in the same plane. Figure S1 illustrates the unfolding process for one vertex, D. The new location D' of the vertex D is calculated as

$$\vec{E_D D'} = \vec{CE_C} \frac{|\vec{E_D D}|}{|\vec{CI}|}.$$

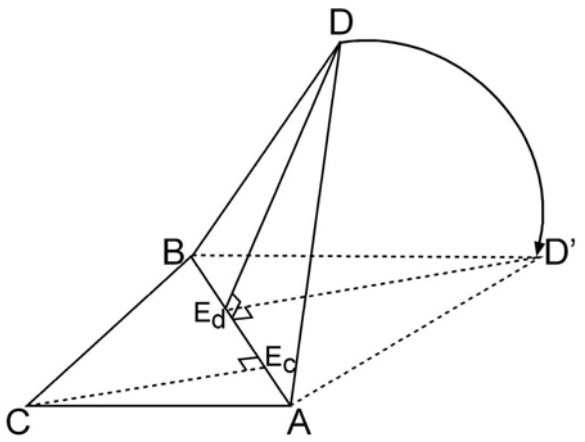

Figure S1. Scheme illustrating the unfolding of two adjoining, triangular faces of a polytope—ABC and ABD—by mapping the point D to point D' in the plane of the triangle CAB.

We modified some routines of the software package so that we could specify the positions of the cuts, and avoid mistakes during the unfolding process. First, we created a polytope approximating a sphere. Figure S2 shows three stages of the unfolding of this polytope into a 2D pattern comprising six segments (flower-petal cut, see Fig. 2e, g of the main text). The unfolding started by selecting one polygon as a center and

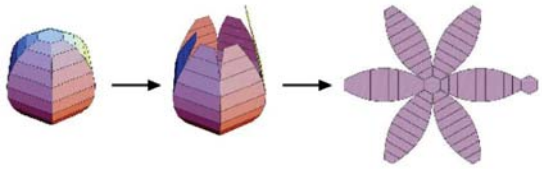

Figure S2. Scheme illustrating three stages of unfolding of a polytope approximating a sphere into a flat surface shaped as the flower-petal cut.

specifying radial cuts away from it. A tree of faces was thus generated, with the central polygon located at the top and faces at the ends of the cuts located at the bottom of the polytope. The polygons were then unfolded as shown in Figure S2.

2. Estimation of the elastic and magnetic free energy of the folded structures. In this estimate we considered the folding of a sphere from a precursor shaped as the equatorial cut (see Fig. 2a, b of the main text).

To estimate the elastic energy of the system, as a first approximation we considered only the bending energy U_b needed to bend a sheet of thickness h made of a material with Young's modulus E into a cylinder using magnets of length R placed in the middle of the segments. Thin elastic sheets are most easily folded by isometric bending of the middle surface, without stretching it[2]; here, we ignored the contribution of the stretching energy which arises due to the presence of boundary layers at ridges[3,4] and peaks[5,6]. Thus, the elastic energy scales as

$$U_b \sim Eh^3\kappa^2 A \qquad (1),$$

where $\kappa \sim 1/R$ is the local mean curvature at the center of the sheet, and $A \sim R^2$ is its area. The elastic energy due to bending alone is largely independent of the radius of the sphere.

To estimate the magnetic energy of the system, we approximated the magnetic field generated by permanent magnets of length L (proportional to the radius of the sphere) and square cross-section b with the field generated by a finite, current-carrying solenoid[7]. The magnetic field $B_{isolated}$ inside each isolated magnet in the unfolded configuration can be described as the magnetic field along the axis of the finite solenoid:

$$B_{isolated} \sim M_0 \left(\frac{z}{\sqrt{z^2 + b^2}} - \frac{z - L}{\sqrt{(z - L)^2 + b^2}} \right) \tag{2},$$

where M_0 is the magnetic strength of the material, z is the distance from the point at which we measure the field to the face of the solenoid, L is the length of the solenoid, and b is its radius (proportional to the width of the magnets). To estimate the magnetic field B_{ring} of the folded configuration, we made the approximation that the magnetic field inside the ring of magnets is constant (similar to the field inside a solenoid torus); thus, it can be expressed[7] as

$$B_{ring} \sim 2M_0 \tag{3}.$$

Using equations (2) and (3), we can express the change of the magnetic energy U_m between the unfolded and the folded configurations as

$$U_m \propto M_0^2 \int_V B_{ring}^2 - B_{isolated}^2 \, dV \tag{4},$$

where the integration is done over the volume V of the magnets. We calculated the magnetic energy difference due to folding numerically, for the limiting case of $L >> b$, as

$$U_m \propto M_0^2 \int_V B_{ring}^2 - B_{isolated}^2 \, dV \propto M_0^2 b^3 \tan^{-1}\left(\frac{L}{b}\right) \tag{5}.$$

This rough estimation of the magnetic energy ignores the shape of the closed ring of magnets (in the structures considered in this work, the ring is shaped as a polygon and not as a circle), the variation of the magnetic field away from the main axis of the solenoid, and the magnetic energy outside the volume of the magnets. Nevertheless, the scaling of the magnetic energy with the dimensions of the magnets is largely independent of these effects.

Using equations (1) and (5), we can then express the balance of the magnetic and elastic energies as

$$\frac{U_m}{U_b} \propto \frac{M_0^2 b^3 \tan^{-1}\left(\frac{L}{b}\right)}{Eh^3 \kappa^2 A} \qquad (6).$$

It is readily apparent that the ratio U_m/U_b depends on the ratios M_0^2/E, b/h, and L/b. The ratio M_0^2/E describes properties of the materials used (magnets and elastic sheets), and does not depend on the dimensions of the folded structure. Using the ratios b/h and L/b, we can estimate how changing the dimensions of the components and the thickness of the elastic membrane will affect the stability of a folded structure: if the width and the length of the magnets are rescaled by a factor α, the thickness of the elastic sheet must be rescaled by the same factor in order to preserve the balance of the two energies, and thereby, the stability of the folded structure.

An important factor that this simple calculation does not take into account is the possibility of co-existence of several stable, folded shapes for a given set of parameters. The next step in refining the scaling estimate will include studies of the energy landscape of the folded structures and the kinetics of the folding process.

3. Finite-element simulation of magnetic field profiles. We performed a finite-element simulation of the two-dimensional magnetic field profiles of the unfolded flat

precursors and of cross-sections of the folded 3D structures using the software package *Finite Element Method Magnetic*[8]. We set the magnetic field intensity at the surface of each magnet to 0.04T (the experimentally measured upper limit), and treated the PDMS membrane as a diamagnetic material with the magnetic characteristics of air (a pre-set feature of the software). From an input of the shape of the flat sheet (or a cross-section of the 3D structure) patterned with magnetic features of given shape, polarity, and magnetic permeability, this software calculates and maps the magnetic field intensity and the magnetic field lines. In the output of the simulation, the intensity of the magnetic field is depicted by color intensity: higher field intensity corresponds to a darker shade of grey. The strength of the interactions between the patterned magnets can be estimated from the strength of the magnetic field and the number of field lines in the space surrounding the magnets. Thus, a magnetic energy minimum corresponds to a map in which the field intensity and the field lines are confined only to the regions of high magnetic permeability (i.e., within the magnets) and do not extend (or extend only to a negligible degree) into the regions of low magnetic permeability (i.e., in the plane of the elastomeric membrane, outside of the magnets).

Figure S3 shows the results of the simulation. In the unfolded equatorial cut (Fig. S3a), there were significant interactions between adjacent magnets positioned in the middle of the segments. No interactions were observed between the magnets positioned at the tips of the segments, and between magnets positioned in the middle and at the tips of each segment. In the unfolded flower-petal cut (Fig. S3b), there was appreciable interaction between the magnets positioned in the middle of the segments. The central region containing six triangular magnets formed a completely closed ring of magnetic dipoles, and showed no stray field lines extending away from the magnets. There was no interaction between magnets positioned at the tips of adjacent sections of the membrane; there was also no interaction between those magnets and the magnets positioned in the middle of the segments. Upon folding of both the equatorial cut and

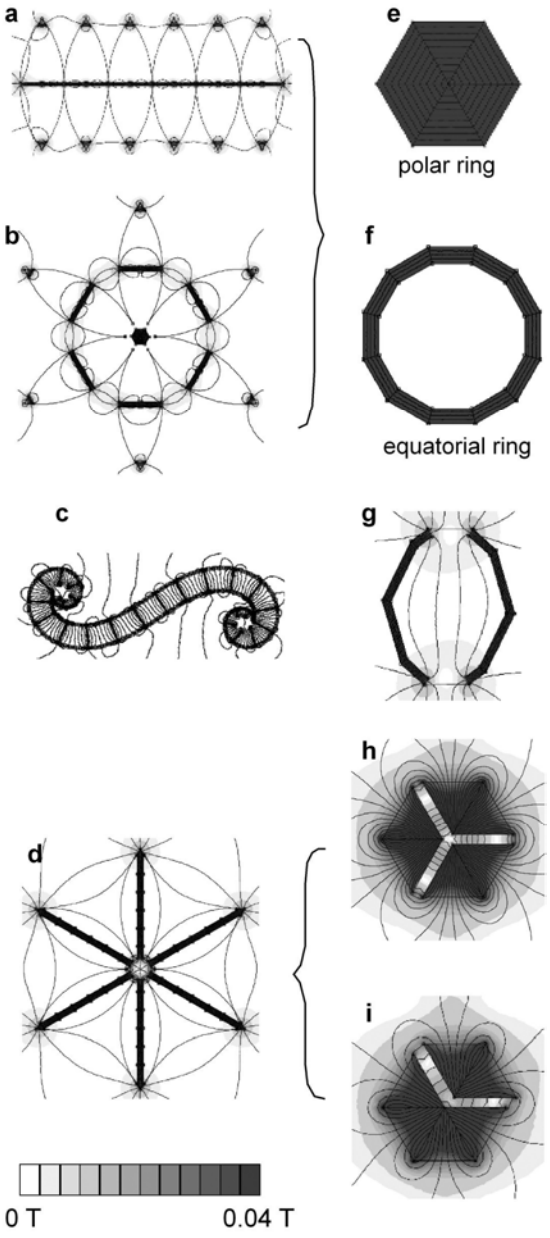

Figure S3: Results of the finite-element simulation of magnetic field profiles of unfolded, flat patterned sheets (a-d) and cross-sections of the corresponding folded 3D structures (e-i). The magnetic field intensity is represented by the color intensity: higher intensity corresponds to darker shade of grey. The scheme is not to scale.

the flower-petal cut, the magnets positioned in the middle of the segments (Fig. S3e) and the magnets positioned at the tips of the segments (Fig. S3f) formed continuous, closed rings of magnetic dipoles; the field intensity and the field lines in these areas were confined exclusively within the rings, indicating minimized magnetic energy of the folded structures.

In the orange-peel cut (Fig. S3c), the simulation showed interactions only between magnets positioned at the two ends of the sheet. In a vertical cross-section of the folded structure (Fig. S3g), the simulation indicates the presence of an overall net dipole moment between the two poles.

The flower-petal cut patterned with magnets arranged anti-parallel to one another (Fig. S3d) did not form a sphere; it folded instead into stable structures comprising groups of two or four petals (see Fig. S2h in the main text). Figures S3h and S3i show simulations of an aggregate comprising three pairs of magnetized features and an aggregate comprising one pair and a group of four magnetized features, respectively. These aggregates correspond to cross-sections of the polar regions of a sphere formed from the flower-petal cut shown in Fig. S3d, in which the groups of two or four magnetized features are separated by a gap of 400 μm. The simulation shows that the field intensity in these gaps is very low or equal to zero; the dipoles aggregated in pairs or in a group of four have formed closed, (magnetically) stable loops. The energy gain of bringing these small loops into a single loop comprising all six segments would be insignificant compared to the energy gain in the case of a flower-petal cut patterned with equatorially magnetized features (as the one shown in Fig. S3c).

4. Fabrication and self-assembly procedures. Figure S4 summarizes our fabrication strategy, illustrated for a membrane having the equatorial cut (see Fig. 2a, b of the main text). We spin-casted (spin conditions: 25 s at 470 rpm) the polymer

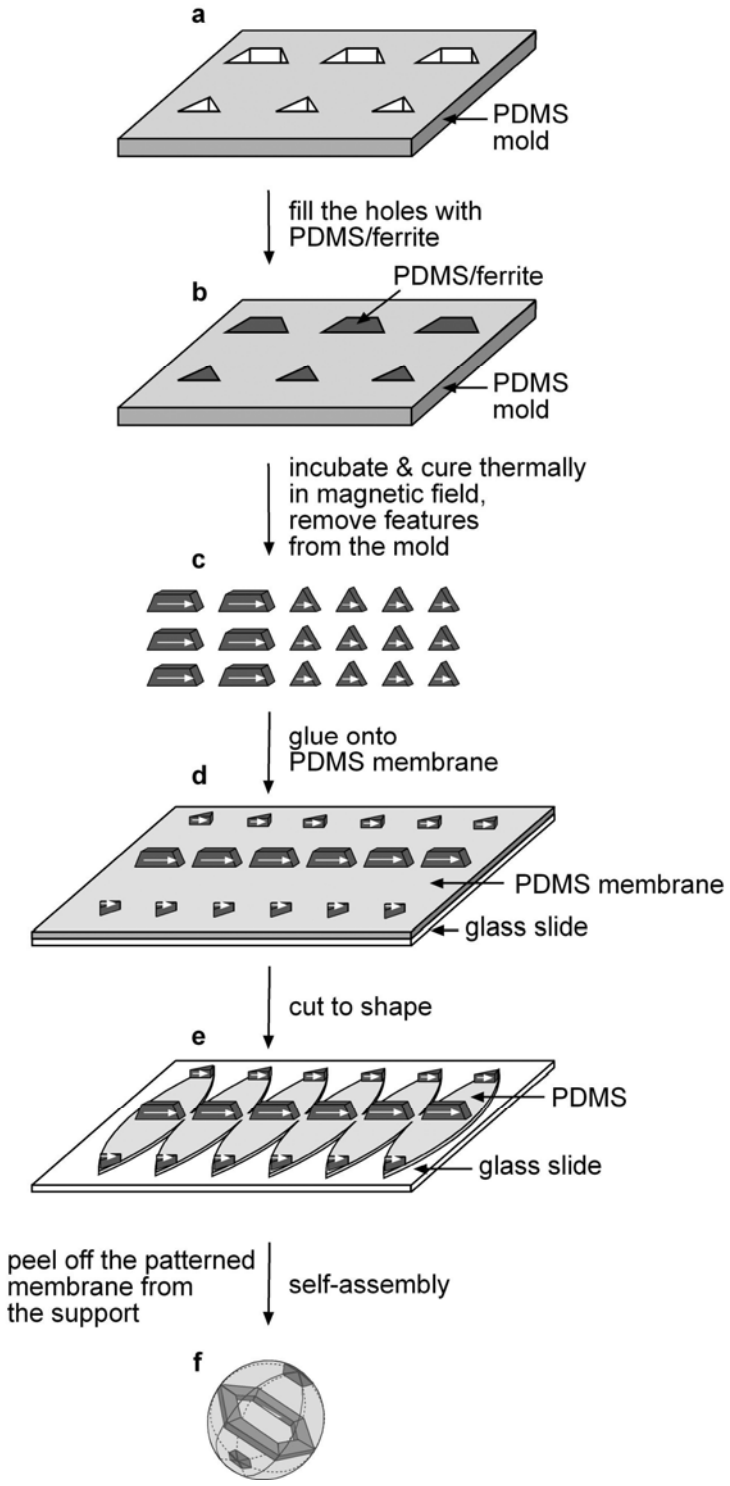

Figure S4: Fabrication and self-assembly of a planar, elastomeric sheet patterned with magnetized features. See text for details.

precursor (Sylgard 184 from Dow Corning, http://www.dowcorning.com) against glass slides treated with (tridecafluoro-1,1,2,2-tetrahydrooctyl)-1-trichlorosilane (United Chemical Technologies, Inc., http://www.unitedchem.com) vapor[9]. The prepolymer was thermally cured for at least 2 hours at 60 °C; the thickness of the resulting PDMS membranes was 240 μm. To fabricate the magnetized features, we used the procedures of soft lithography as previously described[9]. Briefly, we prepared PDMS molds containing holes shaped as right, regular, triangular prisms and truncated, right, rectangular pyramids using replica molding (Fig. S4a). The depth of the holes—corresponding to the thickness of the magnetized features—was one millimeter. After silanizing the molds as described above, we filled the holes with PDMS prepolymer containing approximately 70% (w/w) ferrite powder (Hoosier Magnetics, Inc., http://www.hoosiermagnetics.com), and covered the molds with silanized glass slides (Fig. S4b). We incubated these filled molds for 2 hours in a magnetic field generated between two Nd-Fe-B magnets (residual induction 1.23×10^4 G, from Master Magnetics, Inc., http://www.mastermagnetics.com), and, without removing the molds from the magnetic field, thermally cured the prepolymer for at least 2 hours at 60 °C. Incubation and thermal curing of the PDMS/ferrite mixture in the magnetic field induced 0.03—0.04 T magnetic dipoles in the features; the orientation of these dipoles corresponded to the orientation of the features in the magnetic field (Fig. S4c). We attached the magnetized features to the preformed PDMS membranes in the desired pattern manually, using PDMS prepolymer as glue (Fig. S4d). After thermally curing the glue (30 minutes on a hotplate heated to 80 °C), we cut the membranes to shape using a razor blade (Fig. S4e). Self-assembly of the membranes patterned with magnetic dipoles (Fig. S4f) occurred either on peeling the membranes from the support on which they were fabricated, or required agitation while suspended in a container filled with water or while placed at the air/water interface. We performed each self-assembly experiment at least 4 times, with indistinguishable results in all cases.

5. Fabrication and self-assembly of a spherical electrical circuit. Figure S5 summarizes the fabrication procedure. We fabricated a PDMS membrane of thickness 100 μm (spin conditions: 5 s at 500 rpm, followed by 20 s at 1150 rpm) supported on a silanized glass slide, as described in the previous section (Fig. S5a). After exposing the membrane to an oxygen plasma for 5-10 seconds, we deposited on it a 1-nm thick film of titanium (as an adhesion promoter) followed by 15 nm of gold using e-beam evaporation[10]. We defined a pattern of wires and contact pads on the membrane using photolithography with positive photoresist (Shipley 1813 from Shipley Company L.L.C., http://www.rohmandhaas.com) followed by wet etching using commercial gold and titanium etchants (TFA- and TFTN-type, respectively, from Transene, Inc., http://www.transene.com) (Fig. S5b). We dip-coated the wires and the contact pads with solder (LMA117 from Small Parts, Inc., http://www.smallparts.com, melting temperature T_m = 47 °C) as described[11]. Next, we attached six LEDs (BL-HS136-TR from Bright LED Electronics Corp., http://www.brightled.com) onto contact pads defined on each wire using rosin-core solder wire (from Kester, http://www.kester.com) (Fig. S5c). We covered this patterned membrane with a 90-μm-thick layer of PDMS (spin conditions: 5 s at 500 rpm, followed by 20 s at 1270 rpm), which we cured thermally as above (Fig. S5d). We cut the sheet to shape using a razor blade; the cuts were made through the outside edges of the solder pads embedded between the two layers of PDMS, and thus produced four edges of bare solder near the tips of each section (Fig. S5e). On top of the membrane, we attached magnetized PDMS features as described in the previous section (Fig. S5f).

For self-assembly, we suspended the patterned membrane in a container filled with water (adjusted to pH 3 with acetic acid, and containing a drop of detergent Triton X), heated the water to 60 °C on a hotplate, and gently agitated the container with the suspended membrane. The planar membrane folded into a sphere within 1-3 minutes. After self-assembly was complete, we cooled the resulting structure to room

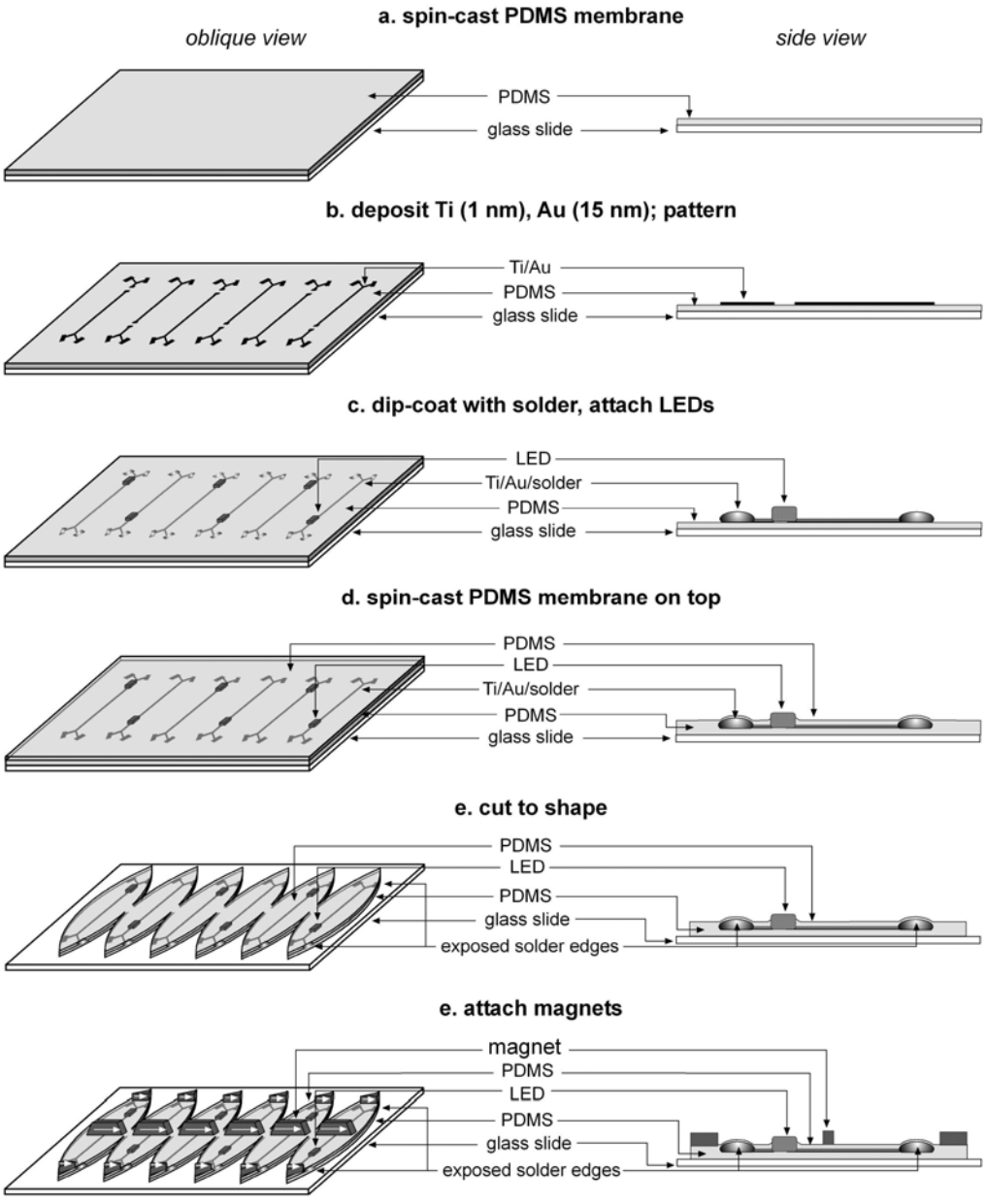

Figure S5. Fabrication of an elastomeric membrane, patterned with magnetized features and containing embedded metal/solder wires and contact pads. The thickness of the layers is not drawn to scale, to emphasize the structure of the sheet. See text for details.

temperature and dried it in air for at least 3 hours. We connected one top and one bottom contact pad to a 3V battery using isolated copper wire (California Fine Wire Company, Inc., http://www.calfinewire.com).

References:

1. Fukuda, K. UnfoldPolytope Mathematica packages. The package we used can be downloaded free from the Internet at http://www.cs.mcgill.ca/˜fukuda/download/mathematica.

2. Rayleigh, J. W. S. *The theory of sound* (Dover, New York, N.Y., 1945).

3. Lobkovsky, A., Gentges, S., Li, H., Morse, D. E. & Witten, T. A. Scaling properties of stretching ridges in a crumpled elastic sheet. *Science* **270**, 1482-1485 (1995).

4. Lobkovsky, A. E. Boundary layer analysis of the ridge singularity in a thin plate. *Phys. Rev. E* **53**, 3750-3759 (1996).

5. Cerda, E. & Mahadevan, L. Conical surfaces and crescent singularities in crumpled sheets. *Phys. Rev. Lett.* **80**, 2358-2361 (1998).

6. Cerda, E., Chaieb, S., Melo, F. & Mahadevan, L. Conical dislocations in crumpling. *Nature* **401**, 46-49 (1999).

7. Purcell, E. M. *Electricity and Magnetism* (McGraw-Hill, New York, N.Y., 1985).

8. The package can be downloaded free from the Internet at http://femm.foster-miller.com.

9. Xia, Y. & Whitesides, G. M. Soft Lithography. *Angew. Chem. Int. Ed.* **37**, 550-575 (1998).

10. Loo, Y.-L. et al. Soft, conformable electrical contacts for organic semiconductors: High-resolution plastic circuits by lamination. *Proc. Natl. Acad. Sci. USA* **99**, 10252-10256 (2002).

11. Gracias, D. H., Tien, J., Breen, T. L., Hsu, C. & Whitesides, G. M. Forming Electrical Networks in Three Dimensions by Self-Assembly. *Science* **289**, 1170-1172 (2000).